Colloids and Surfaces B: Biointerfaces 181 (2019) 567–575

Contents lists available at ScienceDirect

Colloids and Surfaces B: Biointerfaces

journal homepage: www.elsevier.com/locate/colsurfb

Peroxidase mimetic activity of porphyrin modified $ZnFe_2O_4$/reduced graphene oxide and its application for colorimetric detection of H_2O_2 and glutathione

Bing Bian[a,b], Qingyun Liu[b,*], Shitao Yu[a,*]

[a] College of Chemical Engineering, Qingdao University of Science and Technology, Qingdao 266042, China
[b] College of Chemical and Environmental Engineering, State Key Laboratory of Mining Disaster Prevention and Control Co-founded by Shandong Province and the Ministry of Science and Technology, Shandong University of Science and Technology, Qingdao 266590, China

ARTICLE INFO

Keywords:
Porphyrin
$ZnFe_2O_4$
Reduced graphene oxide
Colorimetric
Glutathione

ABSTRACT

Artificial nanoenzymes which can overcome some drawbacks of natural enzymes is a challenging topic in the biosensor field. Herein, we demonstrated 5, 10, 15, 20-tetrakis (4-carboxylpheyl)-porphyrin modified magnetic $ZnFe_2O_4$ nanoparticles loaded on the surface of reduced graphene oxide (Por-$ZnFe_2O_4$/rGO), which exhibited intrinsic peroxidase-like activity and rapidly oxidized the peroxidase substrate 3, 3′, 5, 5′-tetramethylbenzidine (TMB) into a blue product (OxTMB) distinguished by naked eyes. Interestingly, by comparative study of different nanomaterials $ZnFe_2O_4$ nanoparticles, $ZnFe_2O_4$/rGO and Por-$ZnFe_2O_4$, Por-$ZnFe_2O_4$/rGO was proved to possess the highest peroxidase-like activity. Electron spin resonance (ESR) verified the catalytic activity of Por-$ZnFe_2O_4$/rGO for H_2O_2 was due to hydroxyl radical from decomposition of H_2O_2. Temperature and pH strongly affected the peroxidase-like activity of Por-$ZnFe_2O_4$/rGO nanocomposites. Under optimal conditions (pH = 4, 40 °C), the constructed sensor based on the catalytic activity of the Por-$ZnFe_2O_4$/rGO could be conveniently used for colorimetric detection of H_2O_2 in the range of 0.7–30 μM with the detection limit of 0.54 μM. Moreover, the colorimetric sensor based on Por-$ZnFe_2O_4$/rGO exhibited a good linear response to glutathione (GHS) in the range of 2–40 μM with a low detection limit of 0.76 μM. The detection of GHS can be easily realized through the obvious color change by naked eyes without any complicated instrumentation.

1. Introduction

As highly efficient biological catalysts, natural enzymes show high catalytic activity and selectivity in various biochemical reactions [1]. However, they are usually composed of proteins and RNA molecules, which suffer from high cost, poor stability and easy inactivation in harsh conditions and so on. To overcome these drawbacks, artificial nanoenzymes as substitutes for natural ones have been extensively explored in biosensing [2–4], immunoassay [5], cancer treatment [6,7] and pollution treatment [8] recently. Since Fe_3O_4 MNPs was found to possess intrinsic peroxidase-like activity [9], various artificial peroxidase mimics, such as Co_3O_4 [10], V_2O_5 [11], CuO [12], TiO_2 [13] and binary metal oxides $CoFe_2O_4$ [14], $MnFe_2O_4$ [15], $FeWO_4$ [16], $NiCo_2O_4$ [17] have been reported. In previous studies, in order to develop the water solubility, dispersity or biocompatibility, these prepared inorganic nanoparticles were usually modified or coated by polymer [18]. Unfortunately, the catalytic activity of coated inorganic nanoparticles was reduced, owing to decreasing of less active sites. Thus, it becomes an urgent task to prepare different peroxidase mimics with enhanced catalytic activity modified with some functional organic molecules.

As the tetrapyrrole pigments of life, porphyrins (Pors) with an 18 π-electron conjugated system and a highly planar molecular structure, have attracted robust investigations in different fields ranging from photosynthetic antenna models to photodynamic therapy (PDT) due to their unique optical and favorable redox features [19–21]. It is known that porphyrin molecules have been used to modify some inorganic nanomaterials to develop its performances applied in different fields, including photocatalysis [22,23] and sensitized solar cells [24,25]. Some porphyrin compounds have been used in biosensors for its peroxidase-like activity [26,27]. Furthermore, porphyrin functionalized inorganic materials including $CuFe_2O_4$ [28], Fe_3O_4 [29], Co_3O_4 [30], and CeO_2 [31,32], have been found to possess higher catalytic activity than that of pure or bare ones. Nevertheless, spontaneous aggregation

* Corresponding authors.
E-mail addresses: qyliu@sdust.edu.cn (Q. Liu), yushitaoqust@126.com (S. Yu).

https://doi.org/10.1016/j.colsurfb.2019.06.008
Received 23 March 2019; Received in revised form 30 May 2019; Accepted 4 June 2019
Available online 05 June 2019
0927-7765/

and instability of nanoparticles can reduce their catalytic activity greatly and restrict the practical application [33,34]. Hence, researchers have paid attention to employing some supports to anchor inorganic nanomaterials to solve this spontaneous aggregation problem. Spinel $ZnFe_2O_4$ with a relatively narrow band gap of 1.9 eV has been focused on solar transformation, photocatalysis, and hydrogen evolution [35–37], owing to high stability, low toxicity and ease of separation [38–41]. Besides, as a magnetic semiconductor material, $ZnFe_2O_4$ can be magnetically separated from reaction system easily. However, agglomeration inevitably exists in $ZnFe_2O_4$ nanoparticles, which results in the decreasing of catalytic activity.

As a two-dimensional carbon material, graphene nanosheets acts as not only catalysts with intrinsic peroxidase-like activity but also solid supports with high specific surface area, good mechanical strength, excellent electrical conductivity, high chemical and thermal stability [42–44]. Graphene-based nanocomposites, including Co_3O_4/rGO [45] and Fe_3O_4/GO [46] have been reported to exhibit enhanced peroxidase-like activity owning to the synergistic effects between metal oxides and GO or rGO. Based on the idea, if we combine porphyrin modified Spinel $ZnFe_2O_4$ with rGO, the spontaneous aggregation and the poor peroxidase-like activity of $ZnFe_2O_4$ will be solved, due to the introduction of functional porphyrin molecules and the good support rGO.

As we know, porphyrins have lower energy band gap, resulting in the potential application in nanocomposites in favor of electron transfer between different components. Herein, 5, 10, 15, 20-tetrakis(4-carboxylpheyl)-porphyrin modified $ZnFe_2O_4$/rGO (Por-$ZnFe_2O_4$/rGO) was prepared (Scheme 1a). Compared with other sensors based on porphyrin modified nanomaterials [47–49], it was convenient to establish a sensing platform by combining three components together through a simple one-step process. Owing to the strong synergistic effect from porphyrin, $ZnFe_2O_4$ and rGO, Por-$ZnFe_2O_4$/rGO was found to possess superior peroxidase-like activity to rapidly catalyze TMB to be oxidized TMB by H_2O_2 to produce a blue product. A convenient colorimetric sensor based on Por-$ZnFe_2O_4$/rGO was established for rapid, sensitive and selective detection of H_2O_2 and glutathione.

2. Experimental section

2.1. Chemicals

Natural flake graphite powder was purchased from Beijing Creative Biological Engineering Materials. $FeCl_3{\cdot}6H_2O$ and $ZnCl_2$ were bought from Beichen Fangzheng Regent Co. (Tianjin, china). PEG 20,000 and ethylene glycol were purchased from BASF Chemical Co., Ltd (Tianjin, China). Hydrogenperoxide (30 wt%, H_2O_2), sodiumacetate (NaAc), 3, 3′, 5, 5′-tetramethylbenzidine dihydrochloride (TMB·2HCl) and GHS were purchased from Aladdin Chemistry (Shanghai, China). 5, 5-dimethyl-1-pyrroline N-oxide (DMPO) was bought from J&K Chemical Ltd. (Shanghai, china). The medical GSH pills (93.34 wt.%) were purchased from Shandong Luye Pharmaceutical Co., Ltd. All reagents were of analytical grade without further purification. 5, 10, 15, 20-tetrakis(4-carboxylpheyl)-porphyrin (Por) was synthesized according to the previously reported method [50]. All of the solutions have been prepared using hyperpure water (≥18 MΩ, Milli-Q, Millipore)..

2.2. Characterization

The crystallinity of the products were verified by Rigaku D/Max2500PC powder X-ray diffractometer with Cu *Kα* radiation (Rigaku, Japan). The morphology of the samples were analyzed by scanning electron microscopy (SEM, FEI Apreo S) with energy-dispersive X-ray spectrometer (BRUKER XFlash 6160) and transmission electron microscopy (TEM, JEM-2100, JEOL, Japan). And the elemental analysis was performed using Thermo ESCALAB 250Xi Microprobe spectrometer X-ray photoelectron spectroscopy (XPS) with an Al *Kα* incident X-ray beam(Thermo, USA). The quantitative analyses of samples were measured by thermogravimetric analysis (TGA, Netzsch TG 209F1) at 10 °C/min heating rate. Fourier transform infrared spectra (FT-IR) were measured by Thermo Nicolet 8700 spectrometer (Nicolet Thermo, USA). The electron spin resonance (ESR) spectra were performed on a Bruker ESP-300E ESR spectrometer at room temperature (Bruker, Germany). The colorimetric samples were reported on a UV–vis absorption spectrophotometer (UV-1810 PC, Beijing China).

2.3. Preparation of $ZnFe_2O_4$, $ZnFe_2O_4$/rGO, Por-$ZnFe_2O_4$ and Por-$ZnFe_2O_4$/rGO

Graphene oxide was synthesized from natural flake graphite powder by a modified Hummers method according to the previous publication [51]. Por-$ZnFe_2O_4$/rGO was synthesized through a one-step solvothermal method. Typically, GO and 5 mg Por were dispersed in ethylene glycol under ultrasound for 1 h to form a homogeneous suspension. Then $ZnCl_2$ (0.34 g), $FeCl_3{\cdot}6H_2O$ (1.35 g), polyethylene glycol 20,000 (1.0 g) and NaAc (3.6 g) were added into the above suspension under magnetic stirring for another 1 h. The mixture was incubated in a 100 mL teflonlined autoclave at 200 °C for 8 h. After cooling to ambient

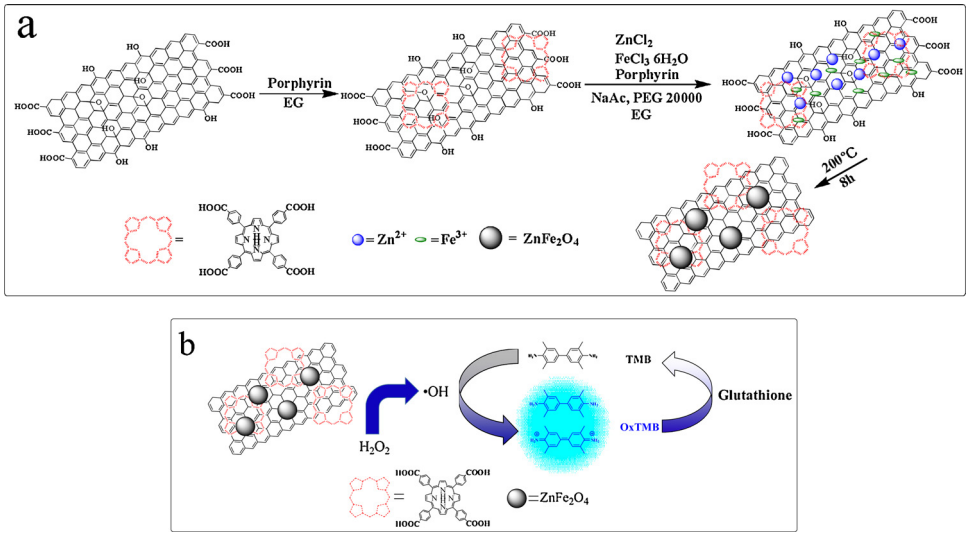

Scheme 1. (a) Schematic illustration of preparation of Por-$ZnFe_2O_4$/rGO and (b) Schematic illustration of peroxidase-like activity of Por-$ZnFe_2O_4$/rGO and colorimetric detection of GHS, respectively.

temperature, the obtained black precipitates were separated by an external magnet and washed three times with ultrapure water and absolute ethanol in turn. Finally, the as-prepared Por-$ZnFe_2O_4$/rGO were dried at 70 °C in a vacuum oven overnight. In addition, in order to comparatively investigate, $ZnFe_2O_4$ nanoparticles, $ZnFe_2O_4$/rGO and Por-$ZnFe_2O_4$ nanocomposites were also synthesized according to the similar method.

2.4. Methods for the peroxidase catalytic activity study

Peroxidase-like activity of Por-$ZnFe_2O_4$/rGO was carried out as follows: firstly, 2 mL acetate buffer solution (pH 4.0) containing 40 μM Por-$ZnFe_2O_4$/rGO, 1 mM TMB, 1 mM H_2O_2 was incubated under visible light at room temperature for 10 min. Then the absorbance of the mixture at 652 nm was recorded. To achieve the best catalytic effect of Por-$ZnFe_2O_4$/rGO, pH values and experimental temperatures were all investigated.

The apparent steady-state kinetic measurements of dynamics were carried out in NaAc-HAc buffer solution (pH 4.0) with different concentrations of H_2O_2 and TMB, respectively. The Michaelis-Menten constant was calculated using the Lineweaver-Burk plots: $1 / \nu = K_m / V_{max} (1 / [S] + 1 / K_m)$, where ν is the initial velocity, V_{max} is the maximum reaction velocity, [S] is the concentration of the substrate and K_m represents the Michaelis-Menten constant.

2.5. Colorimetric detection H_2O_2 and GHS

Colorimetric detection of H_2O_2 was performed as follows: in 1.4 mL sodium acetate buffer solution at pH 4.0, 200 μL of 0.4 mg mL^{-1} Por-$ZnFe_2O_4$/rGO, 200 μL of 10 mM TMB and different concentrations of H_2O_2 was mixed. After incubated under visible light at 40 °C for 10 min, the resultant mixture was used for UV–vis measurement.

GSH was detected using a typical colorimetric analysis as follows: 200 μL Por-$ZnFe_2O_4$/rGO stock solution (0.4 mg mL^{-1}), 200 μL TMB (10 mM), 200 μL H_2O_2 (10 mM) and 200 μL GHS were added into 1200 μL sodium acetate buffer solution (pH 4.0). After incubated under visible light at 40 °C in a water bath for 10 min, the concentration of GHS was determined by the change in $\Delta A (= A_0\text{-}A)$, where A_0 and A are the absorbance values at 652 nm in the absence and presence of GSH, respectively.

To evaluate the selectivity of the proposed method, GHS and different interfering solutions of amino acid samples, electrolytes and glucose were added into the buffer solution containing TMB + H_2O_2 + Por-$ZnFe_2O_4$/rGO. After incubation for 10 min, the absorbance at 652 nm of the mixture was recorded.

For the determination of real GSH sample, commercial GHS tablets were ground into power and dissolved in ultrapure water to form a standard solution. Afterward, the solution was diluted to different concentration for next step. The accuracy of this method can be measured by the recovery and relative standard deviation (RSD) between the determined concentration and the standard concentration.

3. Result and discussion

3.1. Characterization of Por-$ZnFe_2O_4$/rGO

The XRD data of GO and Por-$ZnFe_2O_4$/rGO are presented in Fig. 1a. The diffraction peak at 10.5° can be indexed to (001) plane of GO. The characteristic diffraction peaks of 29.9°, 35.2°, 42.8°, 53.1°, 56.6° and 62.2° can be indexed to (220), (311), (400), (422), (511) and (440) planes of spinel type $ZnFe_2O_4$ (JCPDS 22–1012). However, the typical pattern of GO (001) is not observed in Por-$ZnFe_2O_4$/rGO, indicating that GO was successfully reduced to rGO during the hydrothermal process [43]. The morphology of GO with wrinkled structure is imaged by TEM in Fig. 1b. From Fig. 1c, it can be clearly seen that porphyrin modified $ZnFe_2O_4$ is anchored and well disperses on the surface of rGO. The EDS elemental mapping results are presented in Fig. 1d. From the EDS data, the elements of C, Fe, Zn, O and N were detected, indicating that these elements coexisted in the Por-$ZnFe_2O_4$/rGO nanocomposites.

The thermal stability of the GO and Por-$ZnFe_2O_4$/rGO was tested by thermogravimetric analysis, shown in Fig. S1 (supporting information). Before the tests, all the samples were carefully ground to powders to ensure sufficient diffusion of heat. As shown in curve a, the first weight loss was attributed to the adsorbed water under 100 °C, and the second weight loss from 200 to 300 °C and 300–580 °C attributed major decomposition of oxygen-containing groups and the degradation of the carbon-chain framework [52]. Curve b is the TGA of Por-$ZnFe_2O_4$/rGO. It can be seen the very little weight loss of Por-$ZnFe_2O_4$/rGO adsorbed water under 100 °C. The main loss of Por-$ZnFe_2O_4$/rGO from 250 to 580 °C was attributed to the degradation of the remaining oxygen-containing functional groups of rGO and porphyrin molecules.

XPS was used as a powerful tool to analyze the chemical states of elements. Fig. 2 shows the XPS spectra of Por-$ZnFe_2O_4$/rGO. From Fig. 2a, the peaks of Zn 2p, Fe 2p, O 1s, N 1s and C 1s are observed in the survey spectrum. In detail, two peaks located at 1044.8 eV and 1021.8 eV are rationally ascribed to Zn $2p_{1/2}$ and Zn $2p_{3/2}$ (Fig. 2b), suggesting the oxidation state of Zn^{2+} in the present sample [53,54]. In Fe spectrum, peaks at 711.1 eV and 725.5 eV are ascribed to $Fe_2p_{3/2}$ and $Fe_2p_{1/2}$ (Fig. 2c). The O1 s spectrum displayed in Fig. 2d presents a broad asymmetric curve fitted by two peaks with binding energies at 532.0 eV and 530.3 eV, respectively. The peak at 530.0 eV is assigned to surface lattice oxygen and the other peak at around 532.0 eV is ascribed to surface adsorbed oxygen species such as O^- and O^{2-} [55]. The peaks of C1 s at the binding energies of 284.4 eV, 285.7 eV and 288.6 eV is assigned to the C═C−C, C═N and O−C═O (Fig. 2e). Clearly, it can be observed that the intensity of O−C═O from rGO and porphyrin in Por-$ZnFe_2O_4$/rGO is weaker than the intensity of sp^2 hybridized carbon atom, demonstrating reduction of GO [56]. The peak at 285.7 eV attributing to C═N bonds in Fig. 2e and the peak at 399.9 eV in N1 s (Fig. 2f) spectra regions can prove the existence of the porphyrin molecules in Por-$ZnFe_2O_4$/rGO nanocomposites, because nitrogen element only exists in porphyrin molecules. The structures of GO, porphyrin, $ZnFe_2O_4$/rGO and Por-$ZnFe_2O_4$/rGO were further characterized by FT-IR spectroscopy, shown in Fig. S2 (supporting information).

3.2. Peroxidase-like properties of Por-$ZnFe_2O_4$/rGO

As we know, natural peroxidases can catalyze the oxidation of TMB by H_2O_2 to produce a blue color change observed by naked eyes [9]. Similarly, the peroxidase-like activity of Por-$ZnFe_2O_4$/rGO nanocomposites were investigated using TMB as the chromogenic substrate in the presence of H_2O_2. Fig. S3 (supporting information) displays the absorption spectra and corresponding color change of different systems reacted at 40 °C for 10 min. From Fig. S3, the strongest intensity of absorbance at 652 nm of Por-$ZnFe_2O_4$/rGO + TMB + H_2O_2 reaction system is observed, indicating that Por-$ZnFe_2O_4$/rGO possesses peroxidase-like activity. In addition, it can be seen that the color change of Por-$ZnFe_2O_4$/rGO + TMB is negligible, demonstrating that the Por-$ZnFe_2O_4$/rGO had little catalytic activity in the absence of H_2O_2.

In order to emphasize the peroxidase-like activity of the Por-$ZnFe_2O_4$/rGO nanocomposites, a series of systematical experiments have been designed and carried out. Its activity was compared with those of bare GO, bare $ZnFe_2O_4$, Por-$ZnFe_2O_4$ and $ZnFe_2O_4$/rGO, respectively. As shown in Fig. 3, the Por-$ZnFe_2O_4$/rGO catalyzed the oxidation of TMB by H_2O_2 to produce the deepest blue color observed by naked eyes, which was consistent with that of strongest intensity of absorbance (curve f in Fig. 3). It is suggested that Por-$ZnFe_2O_4$/rGO demonstrated the highest catalytic activity in comparison with that of GO, $ZnFe_2O_4$, Por-$ZnFe_2O_4$ and $ZnFe_2O_4$/rGO.

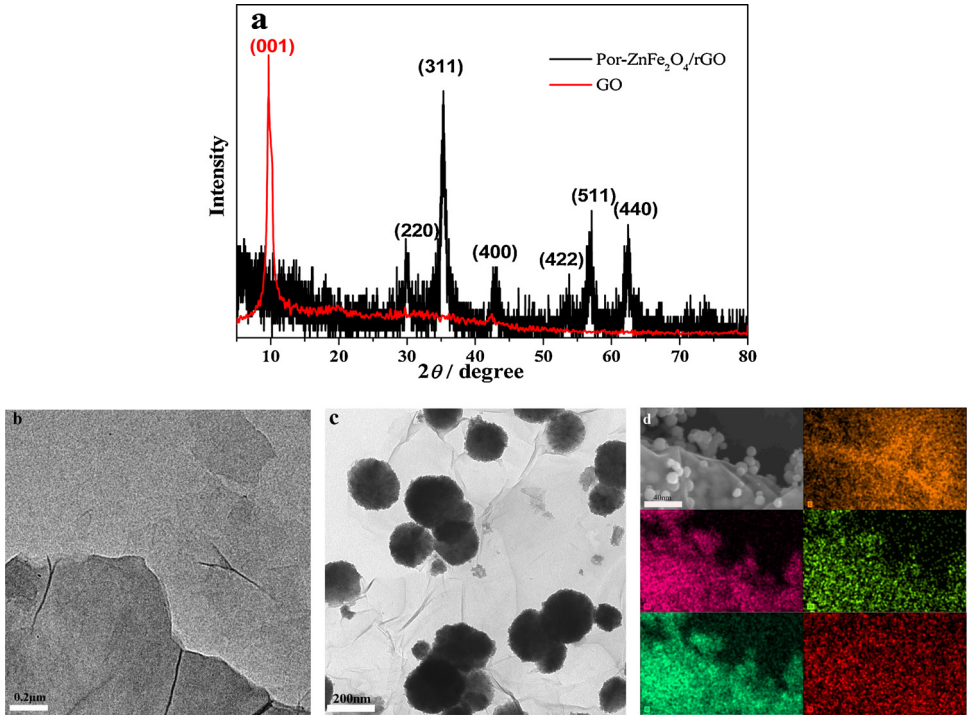

Fig. 1. XRD patterns of GO and Por-$ZnFe_2O_4$/rGO (a), TEM images of GO (b), Por-$ZnFe_2O_4$/rGO (c) and the element mapping (d), respectively.

3.3. Optimization of experimental conditions

Similar to natural enzymes and other reported nanomaterial-based peroxidase mimetics [9], some conditions, such as pH value and temperature, affected the peroxidase-like activity of Por-$ZnFe_2O_4$/rGO. The influence of pH value was studied in the range from 2.0 to 9.0. As shown in Fig. S4a (supporting information), Por-$ZnFe_2O_4$/rGO reached the maximum catalytic activity in acidic environment. As we know, hydrogen peroxide would readily be decomposed into water and oxygen in the basic condition, resulting in the decreasing of hydroxyl radical from hydrogen peroxide. Under pH 4.0, temperature influence on the catalytic activity of Por-$ZnFe_2O_4$/rGO was also investigated at the range of 20–80 °C (Fig. S4b, supporting information). It was found that the catalytic activity of Por-$ZnFe_2O_4$/rGO reached the maximum at 40 °C and then decreased slowly after 40 °C. Therefore, pH 4.0 and 40 °C were chosen as the optimum reaction conditions for subsequent experiments.

3.4. Kinetic studies of the peroxidase-like activity of Por-$ZnFe_2O_4$/rGO

To get further insight into the peroxidase-like behavior of Por-$ZnFe_2O_4$/rGO, the kinetic study was conducted under the optimal conditions (pH 4.0 and 40 °C). The kinetic data were obtained by varying the concentration of TMB or H_2O_2 with a fixed concentration of Por-$ZnFe_2O_4$/rGO. As shown in Fig. 4, it is observed that the oxidation reaction of TMB in the presence of H_2O_2 catalyzed by Por-$ZnFe_2O_4$/rGO followed the typical Michaelis-Menten behaviors toward both TMB and H_2O_2.

As an important criteria for enzymes, Michaelis–Menten constants (K_m) is considered as an indicator of enzyme for substrate which also affects the reaction rate. The lower value of K_m means a stronger affinity. In this work, the K_m of Por-$ZnFe_2O_4$/rGO with H_2O_2 and TMB as substrates were 0.06 mM and 0.117 mM, respectively. Obviously, it can be found that K_m values of Por-$ZnFe_2O_4$/rGO with both H_2O_2 and TMB as substrates are much smaller than that of reported HRP [9] and some nanomaterials with the peroxidase-like activity listed in Table S1. The results suggest that Por-$ZnFe_2O_4$/rGO had a significantly higher affinity for H_2O_2 and TMB, due to the large surface area of rGO with a strong adsorption ability to TMB and H_2O_2.

3.5. Catalytic mechanism of Por-$ZnFe_2O_4$/rGO

According to the previous studies, the catalytic mechanisms of peroxidase mimetic are classified as electron transfer mechanism and radical mechanism [10,57,58]. To study the catalytic mechanism of Por-$ZnFe_2O_4$/rGO, ESR technique was adopted to verify the generation of •OH captured by DMPO as a spin trap. The process was performed in the H_2O_2/UV/DMPO system in the presence and the absence of Por-$ZnFe_2O_4$/rGO. Samples containing 10 mM H_2O_2, 18 mM DMPO and different concentrations of Por-$ZnFe_2O_4$/rGO were prepared in NaAc buffer (20 mM, pH 4.0). After UV irradiated at 365 nm at room temperature for 10 min, each of samples was placed in the ESR cavity for spectrum record. Fig. S5 (supporting information) shows a typical 4-fold characteristic peak of DMPO/•OH spin adduct with relative signal intensity of 1:2:2:1 in the presence of Por-$ZnFe_2O_4$/rGO. It can also be seen that ESR signal intensity of DMPO/˙OH spin adduct increases with the increasing of Por-$ZnFe_2O_4$/rGO. It indicated the O—O bond of H_2O_2 absorbed by Por-$ZnFe_2O_4$/rGO was broken into highly reactive ˙OH, which oxidized TMB into a typical blue color. As a result, it was verified that the peroxidase-like activity of Por-$ZnFe_2O_4$/rGO actually originated from •OH radical generation.

According to the results in our work and some reports [59,60], the mechanism of peroxide-like activity of Por-$ZnFe_2O_4$/rGO was proposed and illustrated in Scheme 2. Each component played important role in the catalytic system. Because porphyrin is a kind of π-conjugated aromatic molecules, electrons are excited from its highest occupied molecular orbital (HOMO) to lowest unoccupied molecular orbital (LUMO) under visible light irradiation easily [29–32], then the electrons further were transferred to the conduction band (CB) $ZnFe_2O_4$. Simultaneously, as we know, graphene sheets are known as good electron acceptors [61]. Thus, the electrons from porphyrin and $ZnFe_2O_4$ are quickly transferred to the surface of rGO [62,63]. As a result, the synergistic effect among porphyrin, $ZnFe_2O_4$ and rGO accelerated the electron transfer, which resulting in the fast decomposition of H_2O_2, and then

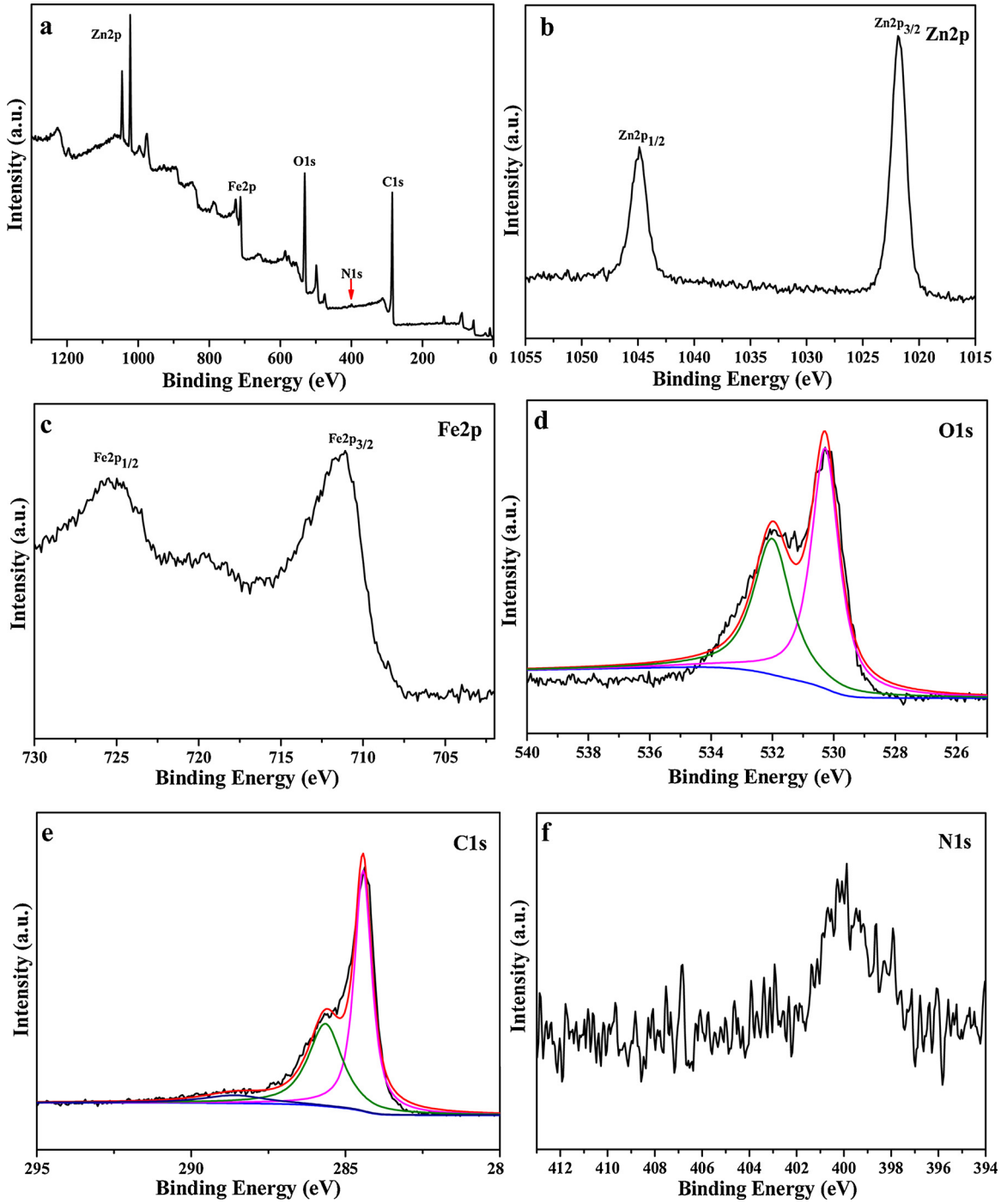

Fig. 2. XPS spectra of Por-$ZnFe_2O_4$/rGO: survey spectrum(a), Zn2p(b), Fe2p(c), O1 s(d), C1 s(e) and N1 s(f), respectively.

accelerated the process of oxidation of TMB [64]. In a word, the Por-$ZnFe_2O_4$/rGO nanocomposites exhibited enhanced catalytic activity because of the synergistic effect of different components.

3.6. Detection of H_2O_2 and GHS

On the basis of the enhanced peroxidase-like activity of Por-$ZnFe_2O_4$/rGO, a rapid colorimetric platform for determination of H_2O_2 and GHS was designed. The design principle of the biosensor is described in Scheme 1b. From Fig. 5, it can be seen that the absorbance of oxidized TMB at 652 nm had a good linear relationship in the concentration range of H_2O_2 from 0.7 to 30 μM (R^2 = 0.992). The detection limit (LOD) was calculated to be 0.54 μM (Fig. 5b). The colorimetric method based on Por-$ZnFe_2O_4$ exhibited a reasonable linear range and a lower detection limit of H_2O_2, compared with that of colorimetric sensors based on other nanomaterials listed in Table S2 (supporting information).

As one of the most abundant biothiols in biological organisms, GHS is indispensable of maintaining the reducing environment to defense against many diseases [65,66]. Therefore, GHS detection is an important task. Since GHS could cause the reduction of blue ox-TMB to colorless TMB [67], a sensitive and simple approach for determination of GHS has been fabricated on the basis of the decrease of the absorbance at 652 nm. Fig. 5c shows the corresponding change of UV–vis spectra of the sample containing TMB, H_2O_2, Por-$ZnFe_2O_4$/rGO and GHS. Clearly, we can obtain a good linear relationship between ΔA and

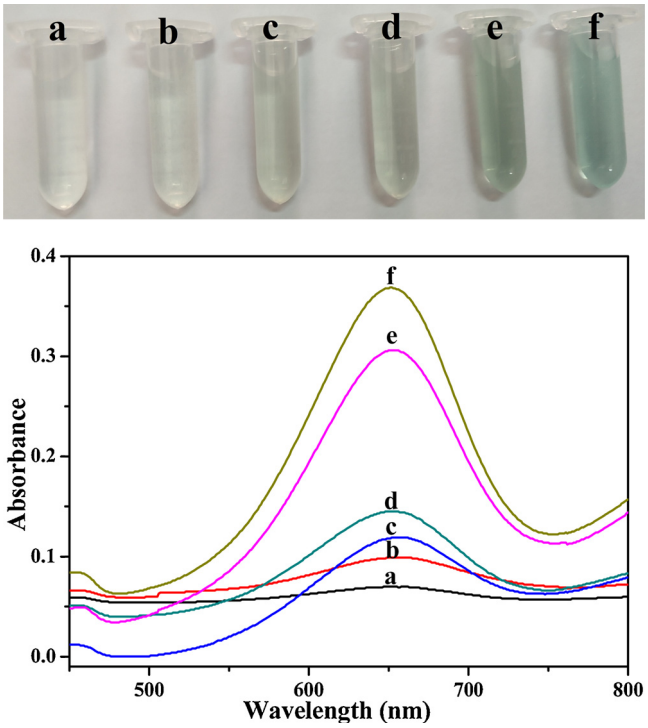

Fig. 3. Typical photographs (top) and UV–vis absorption spectra of TMB-H_2O_2 systems(bottom) in 0.2 M HAc-NaAc buffer at pH 4 incubated at 40 °C for 10 min. (a) TMB + H_2O_2, (b) TMB + H_2O_2 + GO, (c) TMB + H_2O_2 + $ZnFe_2O_4$, (d) TMB + H_2O_2 + $ZnFe_2O_4$/rGO, (e) TMB + H_2O_2 + Por-$ZnFe_2O_4$, and (f)TMB + H_2O_2 + Por-$ZnFe_2O_4$/rGO, respectively.

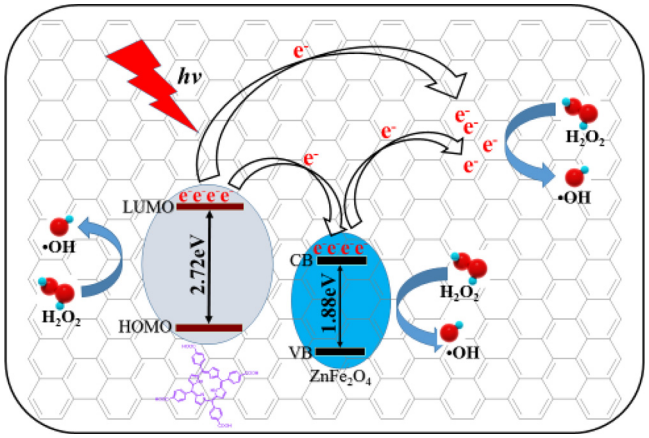

Scheme 2. The possible mechanism of the enhanced peroxide-like activity of Por-$ZnFe_2O_4$/rGO.

the concentrations of GHS from 2 to 40 μM (R^2 = 0.995) with a LOD as low as 0.76 μM ((Fig. 5d). The LOD of the GHS was relatively lower than that of the reported that colorimetric method based on peroxidase-mimics listed in Table S3 (supporting information), as means the sensor based on Por-$ZnFe_2O_4$/rGO is very sensitive toward GHS.

The limit of detection is a key index for evaluating the sensitivity of sensors. In this paper, the LOD of the GSH was relatively lower than that of the reported that colorimetric method based on peroxidase-mimics listed in Table S3 (supporting information). Therefore, it is concluded that the sensor based on Por-$ZnFe_2O_4$/rGO was very sensitive toward GSH. As we know, GSH in our body plays an important role in metabolism, due to the strong ability of capturing free radicals. In this work, Por-$ZnFe_2O_4$/rGO as an excellent peroxidase mimic rapidly

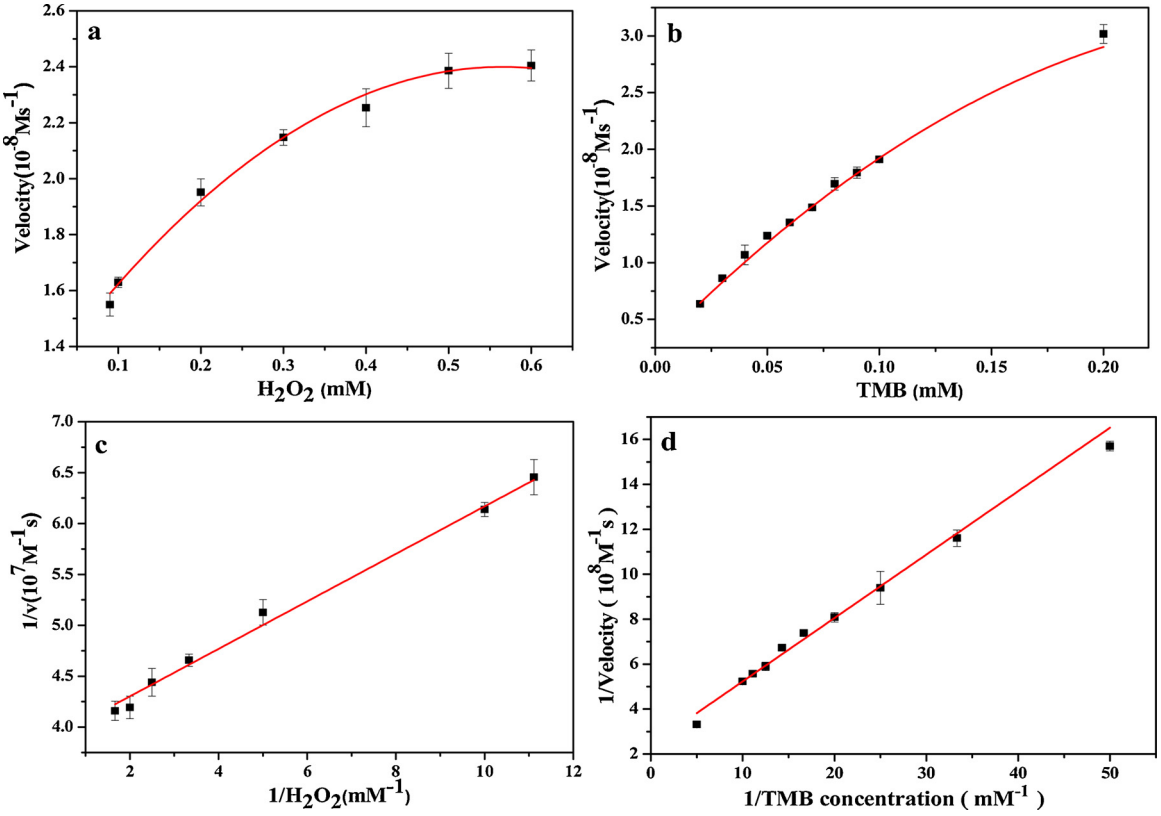

Fig. 4. Steady-state kinetic assay of Por-$ZnFe_2O_4$/rGO. (a) The concentration of TMB is 1 mM and the H_2O_2 concentration is varied. (b) The concentration of H_2O_2 is 10 mM and the TMB concentration is varied, double reciprocal plots of the Michaelis − Menten equation from the activity date of the concentration of H_2O_2 and TMB (c and d). The error bars represent the standard deviation of three measurements.

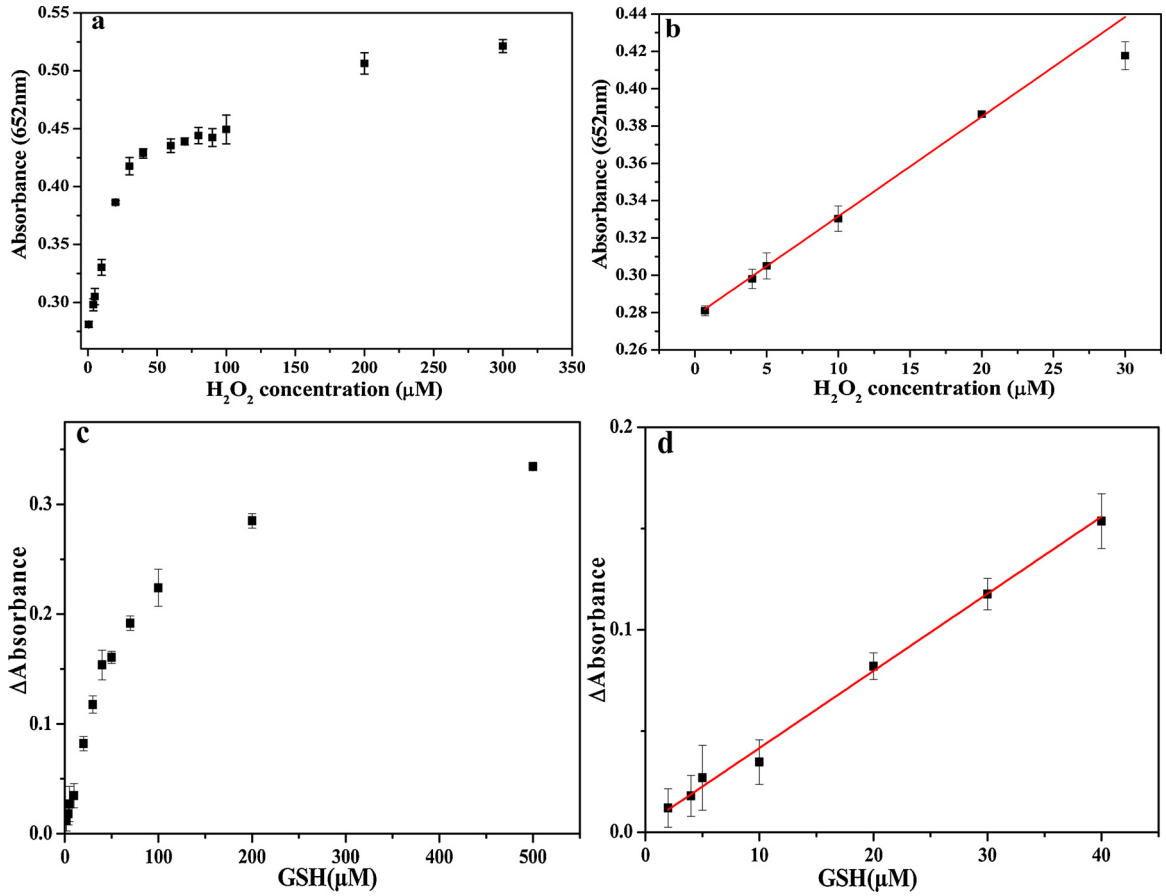

Fig. 5. A dose-response curve for H_2O_2 detection (a) and the linear calibration plot for H_2O_2 detection using Por-$ZnFe_2O_4$/rGO as catalysts (b); A dose-response curve for GHS detection (c) and the linear calibration plot for GHS using Por-$ZnFe_2O_4$/rGO as catalysts (d), respectively. The error bars represent the standard deviation of three measurements.

catalyzed hydrogen peroxide to produce a large number of hydroxyl radical, which were fast captured by GSH existed in the reaction system. Thus, the blue substrate fast fade, which distinguished by the nake eye as well as UV–vis absorption at 652 nm.

To further investigate the selectivity of the colorimetric method for detection of glutathione, we evaluated the interference effects of some components of the pharmaceutical preparation, such as tryptophan (Trp), leucine (Leu), glutamate (Glu), isoleucine (Ile), arginine (Arg), histidine (His), ascorbic acid (AA), serine (Ser), uric acid (UA), Ca^{2+}, K^+, Na^+ and glucose (Gl), respectively. Notably, from Fig. 6a, it can be seen that the absorbance at 652 nm of oxTMB containing GHS was much weaker than that of other saccharides, suggesting that the developed colorimetric method based on the Por-$ZnFe_2O_4$/rGO exhibited high sensitivity and good selectivity in GHS detection. The reusability of the Por-$ZnFe_2O_4$/rGO was also studied in this work. As shown in Fig. 6b, only a slight decline in relative activity was observed after cycling used for 6 cycles. Given the loss of each cycle, the result indicated that Por-$ZnFe_2O_4$/rGO possessed excellent reusability.

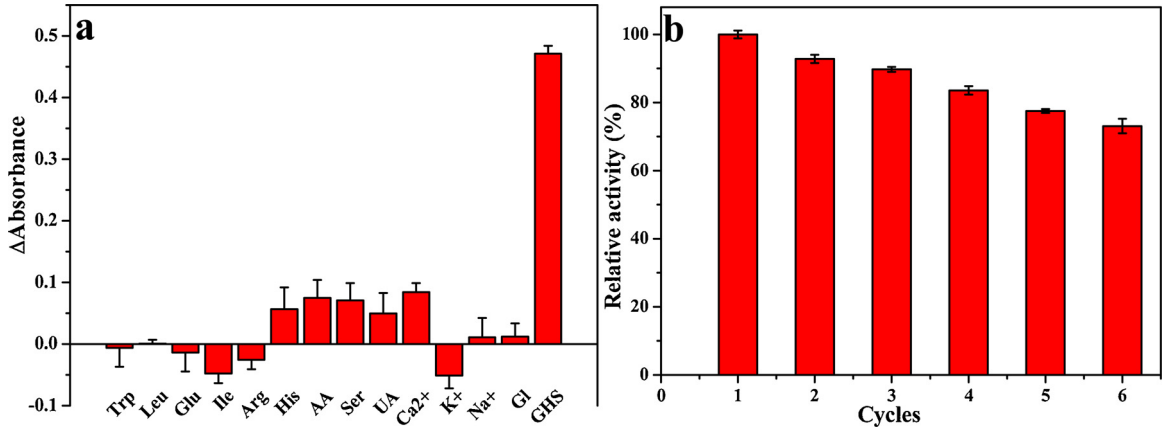

Fig. 6. (a) Selectivity analysis for glutathione detection against several interference substances. The concentrations of glutathione, Tpr, Leu, Glu, Ile, Arg, His, AA, Ser, and UA are 0.5 mM, the concentrations of Ca^{2+}, K^{2+}, Na^{2+} and Gl are 5 mM, respectively. (b) Reusability of Por-$ZnFe_2O_4$/rGO. Error bars stand for the standard deviation of three repeated measurements.

3.7. Analysis of real samples

The feasibility of the assay in real samples was conducted to the determination of GSH in tablet solution by the same method. Herein, the tablet solution was diluted to make sure that the GSH concentration was in the linear range. The recovery values and RSD values were calculated and summarized in Table S4 (Supporting Information). It can be seen that the recovery and RSD were in the range of 95.1%–103.9% and 2.18%–5.49%, respectively. These results indicated that our assay base on Por-$ZnFe_2O_4$/rGO exhibited good reliability for GSH detection in real samples.

4. Conclusion

In summary, Por-$ZnFe_2O_4$/rGO nanocmposites were successfully prepared through a facile one-step method and exhibited enhanced peroxidase-like activity originating from the synergetic effect of different components of Por, $ZnFe_2O_4$ and rGO. The catalytic activity of Por-$ZnFe_2O_4$/rGO was affected by pH and temperature. It is believed that Por-$ZnFe_2O_4$/rGO rapidly catalyze H_2O_2 to be decomposed into •OH, resulting in the rapid oxidation of TMB to form a blue product. Based on the developed peroxidase-like activity of Por-$ZnFe_2O_4$/rGO, a highly sensitive, selective and convenient colorimetric assay for H_2O_2 and glutathione was designed. We anticipate that our work could facilitate the potential applications of Por-$ZnFe_2O_4$/rGO in biotechnology and environmental analysis.

Acknowledgments

This work was supported by National Natural Science Foundation of China (Grant No. 21271119), Natural Science Foundation of Shandong Province (Grant No. ZR2018MB002, ZR2018MEE003), and the Taishan Scholars Construction Projects of Shandong (No. ts201511033).

Appendix A. Supplementary data

Supplementary material related to this article can be found, in the online version, at doi:https://doi.org/10.1016/j.colsurfb.2019.06.008.

References

[1] D.L. Nelson, M.M. Cox, Lehninger Principles of Biochemistry, W. H. Freeman & Co Ltd, New York, 2005.
[2] Y. Lin, J. Ren, X.G. Qu, Catalytically active nanomaterials: a promising candidate for artificial enzymes, Acc. Chem. Res. 47 (2014) 1097–1105.
[3] H. Cheng, L. Zhang, J. He, W. Guo, Z. Zhou, X. Zhang, S. Nie, H. Wei, Integrated nanozymes with nanoscale proximity for in vivo neurochemical monitoring in living brains, Anal. Chem. 88 (2016) 5489–5497.
[4] R. Purbia, S. Paria, Green synthesis of single-crystalline akaganeite nanorods for peroxidase mimic colorimetric sensing of ultralow-level vitamin B1and sulfide ions, ACS Appl. Nano Mater. 1 (2018) 1236–1246.
[5] W. He, Y. Liu, J. Yuan, J.J. Yin, X. Wu, X. Hu, K. Zhang, J. Liu, C. Chen, Y. Ji, Y. Guo, Au@Pt nanostructures as oxidase and peroxidase mimetics for use in immunoassays, Biomaterials 32 (2011) 1139–1147.
[6] S.K. Maji, A.K. Mandal, K.T. Nguyen, P. Borah, Y.L. Zhao, Cancer cell detection and therapeutics using peroxidase-active nanohybrid of gold nanoparticle-loaded mesoporous silica-coated graphene, ACS Appl. Mater. Interfaces 7 (2015) 9807–9816.
[7] S.K. Maji, S.B. Yu, K. Chung, M.S. Ramasamy, J.W. Lim, J.F. Wang, H. Lee, D.H. Kim, Synergistic nanozymetic activity of hybrid gold bipyramid-molybdenum disulfide core@shell nanostructures for two-photon imaging and anticancer therapy, ACS Appl. Mater. Interfaces 10 (2018) 42068–42076.
[8] L.J. Xu, J.L. Wang, Magnetic nanoscaled Fe_3O_4/CeO_2 composite as an efficient fenton-like heterogeneous catalyst for degradation of 4-chlorophenol, Environ. Sci. Technol. 46 (2012) 10145–10153.
[9] L.Z. Gao, J. Zhuang, L. Nie, J.B. Zhang, Y. Zhang, N. Gu, T.H. Wang, J. Feng, D.L. Yang, S. Perrett, X.Y. Yan, Intrinsic peroxidase-like activity of ferromagnetic nanoparticles, Nat. Nanotechnol. 2 (2007) 577–583.
[10] J.S. Mu, Y. Wang, M. Zhao, L. Zhang, Intrinsic peroxidase-like activity and catalase-like activity of Co_3O_4 nanoparticles, Chem. Commun. 48 (2012) 2540–2542.
[11] R. André, F. Natálio, M. Humanes, J. Leppin, K. Heinze, R. Wever, H.C. Schröder, W.E.G. Müller, W. Tremel, V_2O_5 nanowires with an intrinsic peroxidase-like activity, Adv. Funct. Mater. 21 (2011) 501–509.
[12] W. Chen, J. Chen, Y.B. Feng, L. Hong, Q.Y. Chen, L.F. Wu, X.H. Lin, X.H. Xia, Peroxidase-like activity of water-soluble cupric oxide nanoparticles and its analytical application for detection of hydrogen peroxide and glucose, Analyst 137 (2012) 1706–1712.
[13] L.L. Zhang, L. Han, P. Hu, L. Wang, S.J. Dong, TiO_2 nanotube arrays: intrinsic peroxidase mimetics, Chem. Commun. 49 (2013) 10480–10482.
[14] W.B. Shi, X.D. Zhang, S.H. He, Y.M. Huang, $CoFe_2O_4$ magnetic nanoparticles as a peroxidase mimic mediated chemiluminescence for hydrogen peroxide and glucose, Chem. Commun. 47 (2011) 10785–10787.
[15] Y.H. Peng, Z.Y. Wang, W.S. Liu, H.L. Zhang, W. Zuo, H.A. Tang, F.J. Chen, B.D. Wang, Size- and shape-dependent peroxidase-like catalytic activity of $MnFe_2O_4$ Nanoparticles and their applications in highly efficient colorimetric detection of target cancer cells, Dalton Trans. 44 (2015) 12871–12877.
[16] T. Tian, L.H. Ai, X.M. Liu, L.L. Li, J. Li, J. Jiang, Synthesis of hierarchical $FeWO_4$ architectures with {100}-faceted nanosheet assemblies as a robust biomimetic catalyst, Ind. Eng. Chem. Res. 54 (2015) 1171–1178.
[17] L. Su, W.P. Dong, C.K. Wu, Y.J. Gong, Y. Zhang, L. Li, G.J. Mao, S.L. Feng, The peroxidase and oxidase-like activity of $NiCo_2O_4$mesoporous spheres: Mechanistic understanding and colorimetric biosensing, Anal. Chim. Acta 951 (2017) 124–132.
[18] H. Su, D.D. Liu, M. Zhao, W.L. Hu, S.S. Xue, Q. Cao, X.Y. Le, L.N. Ji, Z.W. Mao, Dual-enzyme characteristics of polyvinylpyrrolidone-capped iridium nanoparticles and their cellular protective effect against H_2O_2 induced oxidative damage, ACS Appl. Mater. Interfaces 7 (2015) 8233–8242.
[19] J. Jiang, K. Kasuga, D.P. Arnold, H.S. Nalwa (Eds.), Supramolecular Photosensitive and Electroactive Materials, Academic Press, New York, 2001, pp. 113–210 Chapter 2.
[20] J. Jiang, Advances in Functional Phthalocyanine Materials, Structure and Bonding, Springer-Verlag, Heidelberg, 2010.
[21] Y. Zhang, J. Oh, K. Wang, D. Shin, X. Zhan, Y. Zheng, D. Kim, D. Jiang, The first porphyrin-subphthalocyaninatoboron(III)-fused hybrid with unique conformation and intramolecular charge transfer behavior, Chem. Commun. 52 (2016) 10517–10520.
[22] C.M. Drain, A. Varotto, I. Radivojevic, Self-organized porphyrinic materials, Chem. Rev. 109 (2009) 1630–1658.
[23] Y.Z. Chen, C.Y. Zhang, X.J. Zhang, X.M. Ou, X.H. Zhang, One-step growth of organic single-crystal p-n nano-heterojunctions with enhanced visible-light photocatalytic activity, Chem. Commun. 59 (2013) 9200–9202.
[24] H. Song, Q. Liu, X. Xie, Porphyrin-sensitized solar cells: systematic molecular optimization, coadsorption and cosensitization, Chem. Commun. 54 (2018) 1811–1824.
[25] H. Song, W. Tang, S. Zhao, Q. Liu, Y. Xie, Porphyrin sensitizers containing an auxiliary benzotriazole acceptor for dye-sensitized solar cells: Effects of steric hindrance and cosensitization, Dye. Pigment. 155 (2018) 323–331.
[26] R.A.W. Johnstone, A.J. Simpson, P.A. Stocks, Porphyrins in aqueous amphiphilic polymers as peroxidase mimics, Chem. Commun. (1997) 2277–2278.
[27] T.T. Liu, J. Tian, L. Cui, Q.Y. Liu, L.L. Wu, X.M. Zhang, Facile strategy to prepare a metalloporphyrin-based hydrophilic porous organic polymer with enhanced peroxidase-like activity and high stability for colorimetric detection of H_2O_2 and glucose, Colloids Surf. B Biointerfaces 178 (2019) 137–145.
[28] Z. Xu, X. Lyu, B. Yang, W. Cao, R. Li, X. Zhang, X. Zhang, G. Fan, X. Kong, Q. Liu, Meso-tetrakis(4-chlorophenyl)porphyrin functionalized $CuFe_2O_4/SiO_2$ nanocomposites with enhanced peroxidase-like activity conveniently using for visual biosensing at room temperature, Colloid Surface A 569 (2019) 28–34.
[29] Q.Y. Liu, H. Li, Q.R. Zhao, R.R. Zhu, Y.T. Yang, Q.Y. Jia, B. Bian, L.H. Zhuo, Glucose-sensitive colorimetric sensor based on peroxidase mimics activity of porphyrin-Fe_3O_4 nanocomposites, Mat. Sci. Eng. C 41 (2014) 142–151.
[30] Q.Y. Liu, R.R. Zhu, H. Du, H. Li, Y.T. Yang, Q.Y. Jia, B. Bian, Higher catalytic activity of porphyrin functionalized Co_3O_4 nanostructures for visual and colorimetric detection of H_2O_2 and glucose, Mat. Sci. Eng. C 43 (2014) 321–329.
[31] Q.Y. Liu, Y.T. Yang, X. Lv, Y.N. Ding, Y. Zhang, J. Jing, C. Xu, One-step synthesis of uniform nanoparticles of porphyrin functionalized ceria with promising peroxidase mimetics for H_2O_2 and glucose colorimetric detection, Sensor Actuat. B Chem. 240 (2017) 726–734.
[32] Q.Y. Liu, Y.Y. Ding, Y. Yang, L.Y. Zhang, L.F. Sun, P.P. Chen, C. Gao, Enhanced peroxidase-like activity of porphyrin functionalized ceria nanorods for sensitive and selective colorimetric detection of glucose, Mat. Sci. Eng. C 59 (2016) 445–453.
[33] A. Asati, S. Santra, C. Kaittanis, S. Nath, J.M. Perez, Oxidase-like activity of polymer-coated cerium oxide nanoparticles, Angew. Chem. Int. Ed. 48 (2009) 2308–2312.
[34] S. Wang, W. Chen, A.-L. Liu, L. Hong, H.H. Deng, X.H. Lin, Comparison of the peroxidase-like activity of unmodified, amino-modified, and citrate-capped gold nanoparticles, ChemPhysChem 13 (2012) 1199–1204.
[35] T.W. Hamann, Splitting water with rust: hematite photoelectrochemistry, Dalton Trans. 41 (2012) 7830–7834.
[36] K. Aranishi, H.L. Jiang, K. Akita, K. Haruta, Q. Xu, One-step synthesis of magnetically recyclable Au/Co/Fe triple-layered core-shell nanoparticles as highly efficient catalysts for the hydrolytic dehydrogenation of ammonia borane, Nano Res. 4 (2011) 1233–1241.
[37] K.J. McDonald, K.S. Choi, Synthesis and photoelectrochemical properties of $Fe_2O_3/ZnFe_2O_4$ composite photoanodes for use in solar water oxidation, Chem. Mater. 23 (2011) 4863–4869.
[38] H. Song, L.P. Zhu, Y.G. Li, Z.R. Lou, M. Xiao, Z.Z. Ye, Preparation of $ZnFe_2O_4$ nanostructures and highly efficient visible-light-driven hydrogen generation with the assistance of nanoheterostructures, J. Mater. Chem. A 3 (2015) 8353–8360.
[39] A. Sutka, J. Zavickis, G. Mezinskis, D. Jakovlevs, J. Barloti, Ethanol monitoring by $ZnFe_2O_4$ thin film obtained by spray pyrolysis, Sensor Actuat. B Chem. 176 (2013) 330–334.

[40] J.Q. Wan, X.H. Jiang, H. Li, K.Z. Chen, Facile synthesis of zinc ferrite nanoparticles as non-lanthanide T1 MRI contrast agents, J. Mater. Chem. 22 (2012) 13500–13505.
[41] J. Li, A.R. Wang, Y.Q. Lin, X.D. Liu, J. Fu, L.H. Lin, A study of $ZnFe_2O_4$ nanoparticles modified by ferric nitrate, J. Magn. Magn. Mater. 330 (2013) 96–100.
[42] Z.B. Wang, X.C. Lv, J. Wang, High peroxidase catalytic activity of exfoliated few-layer graphene, Carbon 62 (2013) 51–60.
[43] S.G. Ge, F.F. Lan, F. Yu, J.H. Yu, Applications of graphene and related nanomaterials in analytical chemistry, New J. Chem. 39 (2015) 2380–2395.
[44] Y.S. Fu, X. Wang, Magnetically separable $ZnFe_2O_4$-graphene catalyst and its high photocatalytic performance under visible light irradiation, Ind. Eng. Chem. Res. 50 (2011) 7210–7218.
[45] J.X. Xie, H.Y. Cao, H. Jiang, Y.J. Chen, W.B. Shi, H.Z. Zheng, Y.M. Huang, Co_3O_4-reduced graphene oxide nanocomposite as an effective peroxidase mimetic and its application in visual biosensing of glucose, Anal. Chim. Acta 796 (2013) 92–100.
[46] Y.L. Dong, H.G. Zhang, Z.U. Rahman, L. Su, X.J. Chen, J. Hu, X.G. Chen, Graphene oxide-Fe_3O_4 magnetic nanocomposites with peroxidase-like activity for colorimetric detection of glucose, Nanoscale 4 (2012) 3969–3976.
[47] L. Wu, L.Y. Feng, J.J. Ren, X.G. Qu, Electrochemical detection of dopamine using porphyrin-functionalized graphene, Sensor Actuat. B Chem. 34 (2012) 57–62.
[48] C. Socaci, F. Pogacean, A.R. Biris, M. Coros, M.C. Rosu, L. Magerusan, G. Katona, S. Pruneanu, Grapheneoxide vs. reduced graphene oxide as carbon support in porphyrin peroxidase biomimetic nanomaterials, Talanta 148 (2016) 511–517.
[49] M.J. Lv, T. Mei, C.A. Zhang, X.H. Wang, Selective and sensitive electrochemical detection of dopamine based on water-soluble porphyrin functionalized graphene nanocomposites, RSC Adv. 4 (2014) 9261–9270.
[50] A.D. Adler, F.R. Longo, J.D. Finarelli, J. Goldmacher, J. Assour, L. Korsakoff, A simplified synthesis for meso-tetraphenylporphyrin, J. Org. Chem. 32 (1967) 476.
[51] M. Hirata, T. Gotou, S. Horiuchi, M. Fujiwara, M. Ohba, Thin-film particles of graphite oxide 1:: high-yield synthesis and flexibility of the particles, Carbon 42 (2004) 2929–2937.
[52] X.B. Chen, H. Li, M.F. Chen, W.J. Li, Z.H. Yuan, R. Snyders, Visible-light-driven photocatalytic activities of monodisperse ZnS-coated reduced graphene oxide nanocomposites, Mater. Chem. Phys. 227 (2019) 368–374.
[53] H.J. Lv, L. Ma, P. Zeng, D.N. Ke, T.Y. Peng, Synthesis of floriated $ZnFe_2O_4$ with porous nanorod structures and its photocatalytic hydrogen production under visible light, J. Mater. Chem. 20 (2010) 3665–3672.
[54] L.R. Hou, H. Hua, L. Lian, H. Cao, S.Q. Zhu, C.Z. Yuan, Green Template-free synthesis of hierarchical shuttle-shaped mesoporous $ZnFe_2O_4$ microrods with enhanced lithium storage for advanced Li-Ion batteries, Chem. Eur. J. 21 (2015) 13012–13019.
[55] S.R. Wang, J.X. Zhang, J.D. Yang, X.L. Gao, H.X. Zhang, Y.S. Wang, Z.Y. Zhu, Spinel $ZnFe_2O_4$ nanoparticle-decorated rod-like ZnO nanoheterostructures for enhanced gas sensing performances, RSC Adv. 5 (2015) 10048–10057.
[56] Sun L, R. Shao, L.Q. Tang, Z.D. Chen, Synthesis of $ZnFe_2O_4$/ZnO nanocomposites immobilized on graphene with enhanced photocatalytic activity under solar light irradiation, J. Alloys Comp. 564 (2013) 55–62.
[57] H. Wei, E.K. Wang, Fe_3O_4 magnetic nanoparticles as peroxidase mimetics and their applications in H_2O_2 and glucose detection, Anal. Chem. 80 (2008) 2250–2254.
[58] Y. Gao, C.X. Jin, X.C. Li, K.L. Wu, L.N. Gao, X.T. Lyu, X.X. Zhang, X. Zhang, X.L. Luo, Q.Y. Liu, Two-dimensional porphyrin-Co_9S_8nanocomposites with synergistic peroxidase-like catalysis: Synthesis and application toward colorimetric biosensing of H_2O_2 and glutathione, Colloid. Surface. A 568 (2019) 248–258.
[59] B. Bian, Q.Y. Liu, S.T. Yu, Enhanced peroxidase-like activity of porphyrin functionalized $ZnFe_2O_4$ hollow nanospheres for rapid detection of H_2O_2 and glucose, New J. Chem. 42 (2018) 18189–18200.
[60] D.B. Lu, Y. Zhang, S.X. Lin, L.T. Wang, C.M. Wang, Synthesis of magnetic $ZnFe_2O_4$/graphene composite and its application in photocatalytic degradation of dyes, J. Alloy. Comp. 579 (2013) 336–342.
[61] I.V. Lightcap, T.H. Kosel, P.V. Kamat, Anchoring semiconductor and metal nanoparticles on a two-dimensional catalyst mat. storing and shuttling electrons with reduced graphene oxide, Nano Lett. 10 (2010) 577–583.
[62] M.S. Zhu, Z. Li, B. Xiao, Y.T. Lu, Y.K. Du, P. Yang, X.M. Wang, Surfactant assistance in improvement of photocatalytic hydrogen production with the porphyrin non-covalently functionalized graphene nanocomposite, ACS Appl. Mater. Interfaces 5 (2013) 1732–1740.
[63] N. Khadgi, Y. Li, A.R. Upreti, C. Zhang, W.L. Zhang, Y.M. Wang, D.W. Wan, Enhanced photocatalytic degradation of 17α-ethinylestradiol cxhibited by multifunctional $ZnFe_2O_4$-Ag/rGO nanocomposite under visible light, Photochem. Photobiol. 92 (2016) 238–246.
[64] M. Moshari, M. Rabbani, R. Rahimi, Synthesis of TCPP-Fe_3O_4@S/RGO and its application for purification of water, Res. Chem. Intermed. 42 (2016) 5441–5455.
[65] A. Pompella, A. Visvikis, A. Paolicchi, V. De Tata, A.F. Casini, The changing faces of glutathione, a cellular protagonist, Biochem. Pharmacol. 66 (2003) 1499–1503.
[66] D.M. Townsend, K.D. Tew, H. Tapiero, The importance of glutathione in human disease, Biomed. Pharmacother. 57 (2003) 145–155.
[67] X. Liu, Q. Wang, Y. Zhang, L. Zhang, Y. Su, Y. Lv, Colorimetric detection of glutathione in human blood serum based on the reduction of oxidized TMB, New J. Chem. 37 (2013) 2174–2178.